Research Square

Preprints are preliminary reports that have not undergone peer review.
They should not be considered conclusive, used to inform clinical practice,
or referenced by the media as validated information.

Electronic, optical, and thermal properties of Pd-substituted quasi-two-dimensional C2N2O: A first-principles study

hemn hussein

hemn.hussein@univsul.edu.iq

Research Article

Keywords:

Posted Date: November 18th, 2026

DOI: https://doi.org/10.21203/rs.3.rs-11569553/v1

License: This work is licensed under a Creative Commons Attribution 4.0 International License.
Read Full License

Additional Declarations: No competing interests reported.

Electronic, optical, and thermal properties of Pd-substituted quasi-two-dimensional C_2N_2O: A first-principles study

Hemn Gharib Hussein[1,*], Nzar Rauf Abdullah[2], Vidar Gudmundsson[3]

[1] Physics Department, College of Education, University of Sulaimani, Sulaimani 46001, Kurdistan Region, Iraq.

[2] Division of Computational Nanoscience, Physics Department, College of Science, University of Sulaimani, Sulaimani 46001, Kurdistan Region, Iraq.

[3] Science Institute, University of Iceland, Dunhaga 3, IS-107 Reykjavik, Iceland.

Corresponding author: Hemn Gharib Hussein
Email: hemn.hussein@univsul.edu.iq

Electronic, optical, and thermal properties of Pd-substituted quasi-two-dimensional C_2N_2O: A first-principles study

Hemn Gharib Hussein[a], Nzar Rauf Abdullah[b], Vidar Gudmundsson[c]

[a] *Physics Department, College of Education, University of Sulaimani, Sulaimani 46001, Kurdistan Region, Iraq*
[b] *Division of Computational Nanoscience, Physics Department, College of Science, University of Sulaimani, Sulaimani 46001, Kurdistan Region, Iraq*
[c] *Science Institute, University of Iceland, Dunhaga 3, IS-107 Reykjavik, Iceland*

Abstract

The structural, electronic, optical, and thermal properties of Pd-substituted quasi-two-dimensional (quasi-2D) C_2N_2O are investigated using density functional theory (DFT), together with ab initio molecular dynamics (AIMD) simulations. Three substitutional configurations are considered: Pd replaces a carbon atom in C_2N_2O-1, a nitrogen atom in C_2N_2O-2, and an oxygen atom in C_2N_2O-3. The calculated formation energies are negative for all three configurations, while AIMD simulations indicate that the structures retain their integrity during simulations at 300 K. However, their phonon dispersions contain imaginary-frequency modes, showing that the structures are not dynamically stable within the harmonic approximation. The pristine C_2N_2O structure has an indirect band gap of approximately 2.3 eV. Pd substitution reduces this gap to 0.27, 0.25, and 1.37 eV for C_2N_2O-1, C_2N_2O-2, and C_2N_2O-3, respectively. This reduction is associated with the contribution and hybridization of Pd-4*d* states with the *p* states of the host lattice. The optical response is also strongly dependent on the substitution site: the calculated zero-frequency refractive indices are 2.02, 3.45, and 1.61 for the three configurations, respectively. Their optical-conductivity spectra show corresponding changes in the onset of interband transitions. At 300 K, the calculated heat capacities are approximately 397, 387, and 403 J mol^{-1} K^{-1} for C_2N_2O-1, C_2N_2O-2, and C_2N_2O-3, respectively. These results demonstrate that the electronic and optical properties of quasi-2D C_2N_2O can be modified by selecting the Pd substitution site, although the imaginary phonon modes indicate that further structural stabilization may be required before practical applications are considered.

Keywords:
Density functional theory (DFT), Palladium substitution, Quasi-two-dimensional C_2N_2O, Electronic properties, Optical properties, Heat capacity

1. Introduction

Two-dimensional (2D) materials have attracted extensive research interest because of their distinctive structural, electronic, optical, and thermal properties. These characteristics make them relevant to a range of prospective technologies, including nanoelectronics, thermoelectric systems, and optoelectronic devices. Graphene, a prominent atomically thin material, exhibits high carrier mobility and excellent thermal conductivity. However, its gapless electronic structure limits its direct use in applications that require a finite band gap [1, 2]. This limitation has motivated the investigation of graphene-related and carbon-nitride materials, including C_2N, C_3N_4, and C_3N_5, which have been proposed as semiconducting systems with potentially useful chemical and physical properties [3–7].

The incorporation of oxygen into carbon-nitride frameworks provides an additional route for controlling their bonding characteristics and electronic structures. Carbon–nitrogen–oxygen compounds are therefore of interest because oxygen can modify the local chemical environment and redistribute electronic charge within the host framework [8, 9]. Such changes may also influence orbital hybridization and lattice vibrations, with consequences for the optical and thermal responses of the material [10, 11].

Transition-metal (TM) substitution is widely considered as a means of modifying the electronic and magnetic properties of low-dimensional materials. The partially occupied *d* orbitals of many transition metals can interact strongly with the orbitals of neighboring host atoms, thereby changing the band structure and, in some cases, the magnetic response [12, 13]. Depending on the dopant species and its substitutional site, TM incorporation can alter the semiconducting character of a 2D host or produce other electronic states, including half-metallic behavior [14]. These effects are commonly associated with hybridization between TM-*d* states and the *p* states of the surrounding lattice, which can introduce impurity levels near the Fermi energy and shift the band

Email address: hemn.hussein@univsul.edu.iq (Hemn Gharib Hussein)

edges [15, 16]. Consequently, TM-functionalized materials have been investigated for possible applications in nanoelectronics, spintronics, catalysis, and optoelectronics [17, 18]. In particular, Pd substitution offers a possible means of modifying the electronic structure of carbon-based and other low-dimensional materials.

Previous studies have shown that Pd incorporation can modify the structural and electronic properties of different material systems. Depending on the host material and local chemical environment, Pd doping may affect lattice geometry, defect formation, charge transfer, and the electronic band structure. These changes have been associated with variations in catalytic, electrochemical, photocatalytic, and sensing performance [19–21]. The extent and nature of these effects depend on the position occupied by Pd and its interaction with neighboring atoms.

In the present work, DFT calculations and AIMD simulations are used to examine the structural stability and the electronic, optical, and thermal properties of Pd-substituted quasi-2D C_2N_2O. Three substitutional sites are considered by replacing C, N, or O with a Pd atom. This comparison allows the influence of the local substitution environment on the calculated properties to be assessed. Energetic stability is examined through formation-energy calculations, finite-temperature behavior is investigated using AIMD, and dynamical stability is evaluated from the phonon dispersions. The electronic band structures and projected densities of states are analyzed to identify the orbital contributions associated with the changes in the band gap. The optical response is characterized through the refractive index and optical conductivity, while the temperature dependence of the phonon heat capacity is also evaluated. Particular attention is paid to distinguishing thermal persistence during finite-temperature simulations from dynamical stability inferred from harmonic phonons.

The remainder of this paper is organized as follows. Section 2 describes the structural models and computational methods. Section 3 presents and discusses the stability, electronic, optical, and thermal properties of the Pd-substituted structures. The main findings are summarized in Section 4.

2. Model and Computational Details

The structural models considered in this work are shown in Fig. 1. Panel (a) presents pristine quasi-2D C_2N_2O, while panels (b)–(d) show the three Pd-substituted configurations. In C_2N_2O-1, Pd replaces a C atom; in C_2N_2O-2, it replaces an N atom; and in C_2N_2O-3, it replaces an O atom. The optimized structures distinguish the C, N, O, and Pd atoms using yellow, blue, red, and black spheres, respectively. Structural relaxation produces local changes around the substitutional Pd atom and small distortions of the lattice. Nevertheless, the overall layered framework remains recognizable in all three relaxed configurations. These structures provide the basis for comparing the energetic stability and physical properties associated with the different Pd substitution sites.

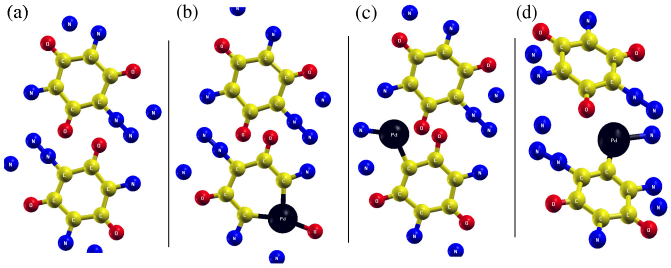


Figure 1: The crystal structure of (a) pure C_2N_2O, (b) C_2N_2O-1, (c) C_2N_2O-2, (d) C_2N_2O-3.

The first-principles calculations are performed within DFT using the Quantum ESPRESSO (QE) package [22, 23]. The exchange-correlation energy is described using the Perdew–Burke–Ernzerhof (PBE) generalized-gradient approximation (GGA) [24]. The quasi-2D C_2N_2O structure is used as the host system. Pd substitution is modeled by replacing a C, N, or O atom, allowing the dependence of the structural, electronic, optical, and thermal properties on the substitutional site to be examined.

A plane-wave kinetic-energy cutoff of 816.3 eV is employed. Structural relaxations and self-consistent-field (SCF) calculations use Monkhorst–Pack k-point meshes of $7\times6\times6$, $14\times12\times12$, and $7\times6\times6$ for C_2N_2O-1, C_2N_2O-2, and C_2N_2O-3, respectively. The density of states (DOS) is calculated using non-self-consistent-field (NSCF) calculations with denser meshes of $21\times18\times18$, $35\times30\times30$, and $21\times18\times18$ for the same three configurations, respectively.

All atomic coordinates are relaxed until the residual forces are below 0.001 eV/Å, with an energy-convergence threshold of 1.4×10^{-4} eV. The converged SCF charge density is then used in the calculations of the electronic band structures and optical spectra. Optical properties are evaluated within the independent-particle approximation (IPA) [25]. Atomic structures are visualized and examined using XCrySDen [26].

Finite-temperature behavior is examined using AIMD simulations in the canonical NVT ensemble with a Nosé–Hoover thermostat set to 300 K. Each simulation is performed for 10 ps using a 1.0 fs time step and a $2\times2\times1$ supercell [27]. Phonon dispersions and phonon-derived thermodynamic properties, including heat capacity, are calculated using PHONOPY [28].

3. Results and Discussion

This section examines how the substitutional position of Pd influences the properties of quasi-2D C_2N_2O. Replacing C, N, or O creates distinct local bonding environments and relaxed geometries. The resulting changes are assessed through energetic and dynamical stability analy-

ses, AIMD simulations, electronic band structures, optical spectra, and phonon heat capacities.

3.1. Stability

The stability of the Pd-substituted structures is assessed using three complementary approaches: formation-energy calculations for energetic stability, phonon dispersions for harmonic dynamical stability, and AIMD simulations for their behavior at finite temperature. These criteria probe different aspects of stability and are therefore considered separately.

Formation energy is used to examine the energetic favorability of the Pd-substituted structures. A negative value indicates that the calculated total energy lies below the chosen set of elemental reference energies. Comparisons between different configurations are meaningful when the same reference conventions and normalization are used [29]. The formation energy per atom is evaluated as

$$E_f = \frac{E_{\mathrm{tot}}(\mathrm{C_2N_2O:Pd}) - N_C\mu_C - N_N\mu_N - N_O\mu_O - N_{\mathrm{Pd}}\mu_{\mathrm{Pd}}}{N_{\mathrm{atoms}}} \tag{1}$$

Here, $E_{\mathrm{tot}}(\mathrm{C_2N_2O:Pd})$ is the total DFT energy of a Pd-substituted unit cell; N_C, N_N, N_O, and N_{Pd} are the numbers of C, N, O, and Pd atoms, respectively; and μ_C, μ_N, μ_O, and μ_{Pd} are the corresponding chemical potentials. The reference chemical potentials are taken from bulk graphite for C, isolated N_2 and O_2 molecules for N and O, and bulk metallic Pd for Pd. N_{atoms} is the total number of atoms in the cell. The calculated formation-energy curves are shown in Fig. 2. Their minima identify the relaxed lattice parameters used in the subsequent calculations.

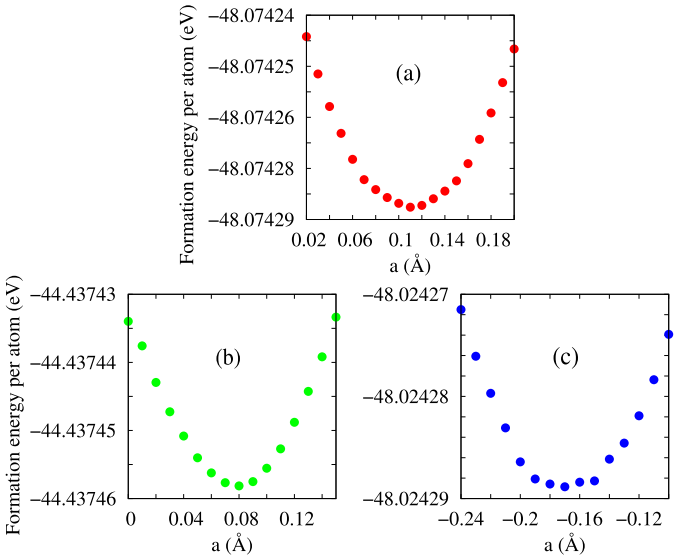


Figure 2: Formation energy per atom of Pd-doped quasi-2D C_2N_2O structures as a function of lattice constants for (a) C_2N_2O-1, (b) C_2N_2O-2, and (c) C_2N_2O-3.

The formation-energy minima obtained for C_2N_2O-1, C_2N_2O-2, and C_2N_2O-3 are −48.07, −44.43, and −48.02 eV, respectively. Among the three Pd-substituted models, C_2N_2O-1 has the lowest reported value, followed closely by C_2N_2O-3, whereas C_2N_2O-2 has a less negative value. The differences are consistent with the distinct local environments created when Pd occupies the C, N, or O site. In particular, the spatially extended Pd-4*d* orbitals can interact differently with the neighboring atoms in each configuration, leading to different degrees of local relaxation and changes in the total energy. The pristine-system value reported in Ref. [30] is −4.72 eV. Because the normalization and reference conventions must be identical for a quantitative comparison, the pristine and substituted values should not be used to rank their relative stability unless this consistency has been verified.

As shown in Fig. 2, the formation energy varies approximately parabolically with the lattice parameter. This behavior is characteristic of a system approaching its equilibrium geometry. Compression below the equilibrium lattice parameter increases short-range repulsion, whereas expansion weakens orbital overlap and bonding interactions. Both effects raise the energy. The minimum of each curve therefore identifies the lattice parameter associated with the lowest calculated energy for that configuration.

The finite-temperature behavior of the three Pd-substituted structures is examined by AIMD simulations in the NVT ensemble at 300 K. Each trajectory extends over 10 ps with a time step of 1.0 fs. Figure 3 shows the temperature and total-energy profiles during the simulations. The temperature fluctuates around the target value, as expected for an NVT trajectory. The total-energy variations remain within approximately 0.9 eV. No pronounced structural reconstruction, bond breaking, or large-scale atomic rearrangement is observed over the simulated interval. Thus, all three configurations retain their structural integrity during the 10 ps simulations at 300 K. This observation indicates finite-temperature persistence on the simulated time scale; it does not, by itself, establish harmonic dynamical stability.

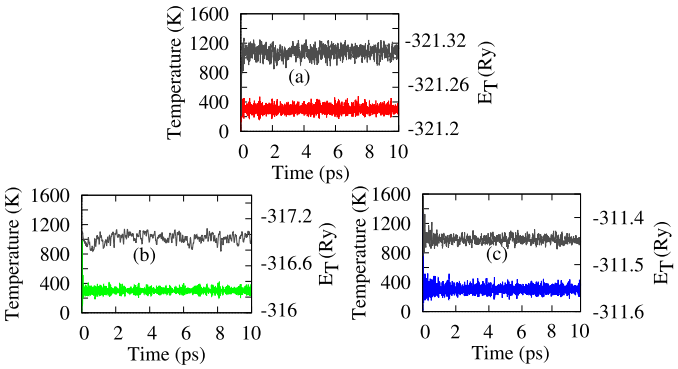


Figure 3: AIMD simulation of Pd-doped quasi-2D C_2N_2O structures at 300 K showing the variation of temperature and total energy E_T as a function of simulation time for (a) C_2N_2O-1, (b) C_2N_2O-2, and (c) C_2N_2O-3.

The phonon dispersions provide a separate test of the

harmonic dynamical stability of the Pd-substituted structures. A dynamically stable structure should have no imaginary phonon frequencies throughout the Brillouin zone; imaginary frequencies indicate modes along which small atomic displacements lower the harmonic energy. As shown in Fig. 4(a)–(c), all three Pd-substituted configurations contain imaginary-frequency branches. They therefore cannot be classified as dynamically stable within the present harmonic phonon calculations. The pristine quasi-2D C_2N_2O structure reported in Ref. [30] exhibits more pronounced imaginary modes, while the Pd-substituted structures show fewer such modes. This comparison suggests a relative reduction in the extent of the imaginary branches after Pd substitution, but does not remove the dynamical instability. The higher-frequency optical branches also differ among the configurations, reflecting their different local bonding environments.

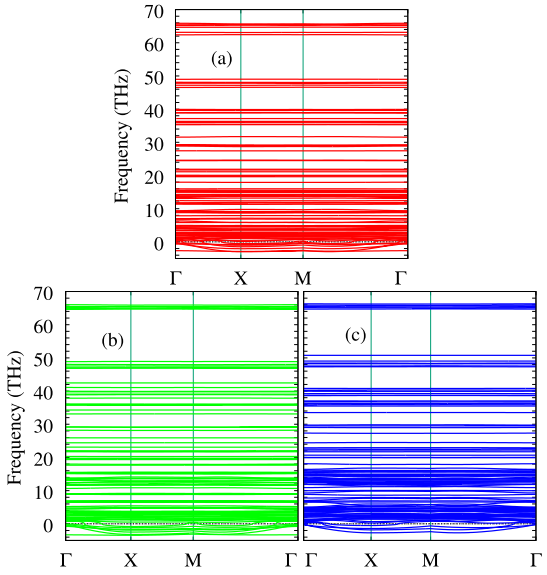


Figure 4: Phonon band structure of Pd-doped quasi-2D C_2N_2O structures: (a) C_2N_2O-1, (b) C_2N_2O-2, and (c) C_2N_2O-3.

3.2. Electronic properties

The electronic band structures of the three Pd-substituted configurations are presented along the selected high-symmetry directions of the Brillouin zone in Fig. 5. The pristine quasi-2D C_2N_2O structure has previously been reported to be an indirect-gap semiconductor with a band gap of approximately 2.3 eV, associated mainly with the C-, N-, and O-2*p* states [30]. Pd substitution substantially changes this electronic structure. When Pd replaces C in C_2N_2O-1, the calculated gap decreases to approximately 0.27 eV. Substitution at the N site in C_2N_2O-2 produces a similarly narrow gap of about 0.25 eV. In contrast, replacing O in C_2N_2O-3 yields a larger gap of approximately 1.37 eV. The results show that the electronic response is strongly dependent on the chemical identity of the substituted host site.

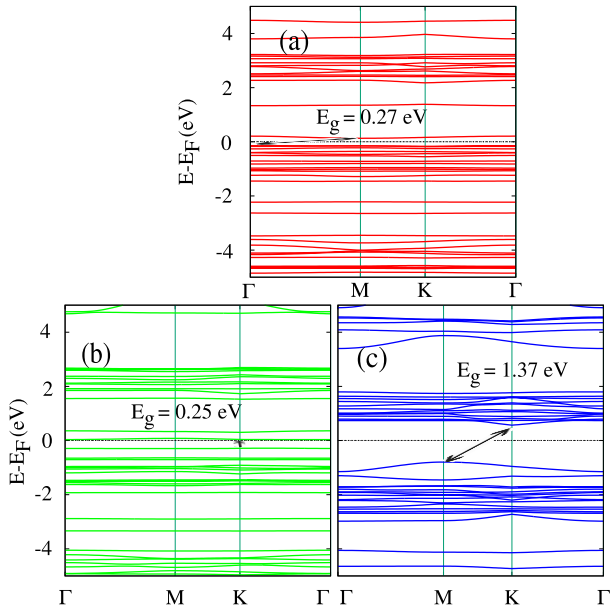


Figure 5: The band structure of (a) C_2N_2O-1, (b) C_2N_2O-2, (c) C_2N_2O-3.

To identify the orbital contributions responsible for the changes in the band structures, the total and projected densities of states (TDOS and PDOS) are analyzed, as shown in Fig. 6. In pristine C_2N_2O, the valence-band maximum (VBM) is dominated by O-*p* states, whereas the conduction-band minimum (CBM) has a substantial N-*p* contribution, as reported in Ref. [30]. The introduction of transition-metal states near the Fermi level can modify the band edges and reduce the band gap through hybridization with the host orbitals [16, 32].

Pd substitution introduces Pd-4*d* contributions close to the Fermi energy and changes the orbital composition of the band edges. The PDOS indicates hybridization between Pd-*d* states and the *p* states of neighboring atoms, thereby introducing additional states within or near the band-gap region. These states alter the positions and character of the valence- and conduction-band edges. In the C_2N_2O-1 and C_2N_2O-2 configurations, the stronger Pd-*d* contribution near the Fermi level is consistent with their narrow calculated gaps. For C_2N_2O-3, the smaller contribution of Pd-derived states near the band edges is consistent with its comparatively larger gap. Thus, the differences among the three band structures can be related to the site-dependent interaction between Pd-4*d* states and the electronic states of the host framework.

3.3. Optical properties

The optical response of the Pd-substituted structures is characterized by the refractive index and optical conductivity. These quantities provide information about the interaction between electromagnetic radiation and the electronic states of the material. The calculated spectra cover photon energies from 0 to 6 eV, spanning the infrared-to-ultraviolet energy range.

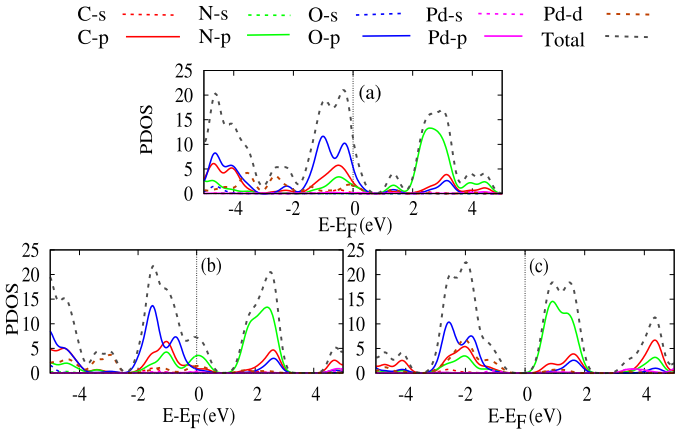


Figure 6: Total density of states (TDOS) and partial density of states (PDOS) for (a) C_2N_2O-1, (b) C_2N_2O-2, and (c) C_2N_2O-3 structures showing the orbital contributions of C, N, O, and Pd atmo near the Fermi level.

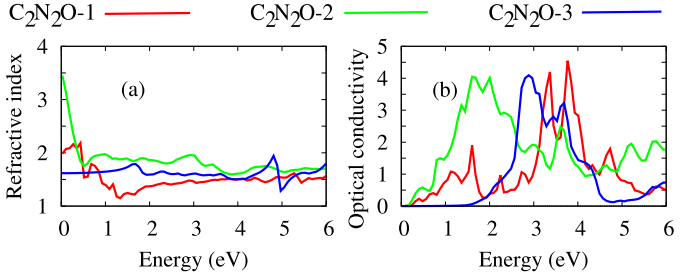


Figure 7: Refractive index (a) and optical conductivity (b) for Pd-doped C_2N_2O structures as a function of photon energy.

Figure 7(a) shows the refractive index $n(\omega)$ as a function of photon energy. The refractive index describes the phase propagation of light in a material and is related to its frequency-dependent dielectric response. The calculated zero-frequency values are 2.02, 3.45, and 1.61 for C_2N_2O-1, C_2N_2O-2, and C_2N_2O-3, respectively. These values differ from the value of approximately 2.1 reported for pristine quasi-2D C_2N_2O [30]. The largest value occurs for C_2N_2O-2, while C_2N_2O-3 has the smallest value. This site dependence is consistent with changes in the electronic polarizability associated with the different Pd–host orbital interactions.

Although C_2N_2O-1 has a lower zero-frequency refractive index than C_2N_2O-2, its value is higher than that of C_2N_2O-3. As the photon energy increases, the refractive index becomes dispersive and develops spectral features associated with transitions between occupied and unoccupied electronic states. The positions and amplitudes of these features depend on the electronic structure of each substitutional configuration.

The optical-conductivity spectra in Fig. 7(b) show the energy-dependent response of the three configurations. The conductivity is small below the onset of allowed interband transitions and increases when the photon energy becomes sufficient to excite electrons from occupied to unoccupied states. The calculated onset energies are approximately 0.26 eV for C_2N_2O-1, 0.24 eV for C_2N_2O-2, and 1.45 eV for C_2N_2O-3. These values are consistent with the corresponding narrow and wider band gaps obtained from the electronic band structures. They are also lower than the approximately 2.3 eV onset reported for pristine quasi-2D C_2N_2O [30]. The reduced onset energies in C_2N_2O-1 and C_2N_2O-2 are consistent with the presence of Pd-4*d* states near the band edges and their hybridization with the host *p* orbitals. At higher photon energies, additional conductivity peaks arise from transitions involving the C-, N-, and O-*p* states and Pd-*d* states.

Taken together, the refractive-index and optical-conductivity results show that Pd substitution modifies the optical response of quasi-2D C_2N_2O. Both the magnitude of the zero-frequency refractive index and the optical-conductivity onset depend on the substitutional site. In particular, substitution at the C and N sites produces lower-energy optical transitions than substitution at the O site. These results indicate that the optical properties can be tuned through the choice of Pd site, although the dynamical stability limitations identified above should be considered when assessing potential applications.

3.4. Thermal properties

The thermal response is examined through the temperature dependence of the phonon heat capacity. Heat capacity measures the thermal energy required to raise the temperature of a system and, within the harmonic approximation, is governed by the population of its vibrational modes [33]. The phonon heat capacities are calculated from the DFT-derived phonon properties using PHONOPY [28, 34].

Figure 8 presents the calculated heat capacity as a function of temperature from 0 to 1000 K for C_2N_2O-1, C_2N_2O-2, and C_2N_2O-3. At low temperatures, the heat capacity rises as the low-energy vibrational modes become populated. In the low-temperature Debye regime, this behavior is commonly described by a T^3 dependence. With increasing temperature, progressively more phonon modes contribute to the thermal response, and the heat capacity approaches its high-temperature limit.

At 300 K, the calculated heat capacities are approximately 397, 387, and 403 J mol^{-1} K^{-1} for C_2N_2O-1, C_2N_2O-2, and C_2N_2O-3, respectively. They increase with temperature and reach approximately 620, 618, and 639 J mol^{-1} K^{-1} at 1000 K. Among the three configurations, C_2N_2O-3 has the largest calculated heat capacity over the reported temperature range, whereas C_2N_2O-2 has the smallest. For comparison, the pristine quasi-2D C_2N_2O structure has a reported heat capacity of approximately 624 J mol^{-1} K^{-1} at 1000 K [30]. The values obtained for C_2N_2O-1 and C_2N_2O-2 are slightly lower, while that of C_2N_2O-3 is somewhat higher. These differences may be associated with changes in the vibrational spectrum and phonon populations caused by the distinct local bonding environments around the substituted Pd atom. Thus, the substitutional site influences the calculated thermal response of the lattice.

The heat capacities normalized per atom at 1000 K are 20.6, 20.6, and 21.3 J mol^{-1} K^{-1} atom^{-1} for C_2N_2O-1, C_2N_2O-2, and C_2N_2O-3, respectively. These values are below the classical Dulong–Petit limit of approximately $3k_B$ per atom, but approach that limit at high temperature. The reported values are comparable to those cited for other carbon- and boron-nitride materials, including d-C_3N_4 and related nitrides [35, 36]. The differences indicate that the vibrational contributions to heat capacity depend on the atomic composition and bonding environment of each structure.

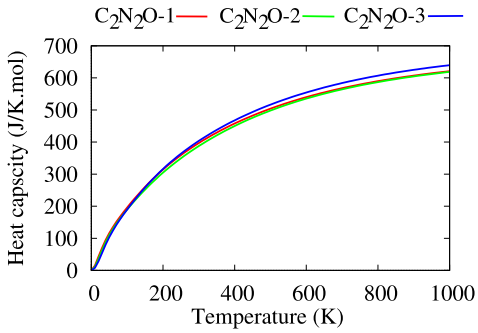


Figure 8: Heat capacity of Pd-doped quasi-2D C_2N_2O structures as a function of temperature for C_2N_2O-1 (red line), C_2N_2O-2 (green line), and C_2N_2O-3 (blue line).

4. Conclusions

DFT calculations and AIMD simulations have been used to investigate the structural stability and the electronic, optical, and thermal properties of Pd-substituted quasi-2D C_2N_2O. Three substitutional configurations were examined, with Pd replacing C, N, or O. The calculated formation energies are negative for all three Pd-substituted models, and the AIMD trajectories show that their structures remain intact during 10 ps simulations at 300 K. However, imaginary-frequency branches are present in the phonon dispersions of all three configurations. The structures therefore exhibit finite-temperature persistence over the simulated time interval but remain dynamically unstable within the harmonic approximation. The pristine material has an indirect band gap of approximately 2.3 eV. Pd substitution reduces the calculated gaps to 0.27 eV for C_2N_2O-1, 0.25 eV for C_2N_2O-2, and 1.37 eV for C_2N_2O-3. The PDOS analysis associates these changes with contributions from Pd-4*d* states and their hybridization with the host *p* orbitals. The optical response also depends on the substitution site: the zero-frequency refractive indices are 2.02, 3.45, and 1.61 for C_2N_2O-1, C_2N_2O-2, and C_2N_2O-3, respectively, while the optical-conductivity onsets occur at approximately 0.26, 0.24, and 1.45 eV. The corresponding heat capacities at 300 K are approximately 397, 387, and 403 J mol^{-1} K^{-1}. Overall, the results show that the electronic and optical properties of quasi-2D C_2N_2O are sensitive to the Pd substitutional site. Further work aimed at removing the imaginary phonon modes is needed before the doped structures can be considered dynamically stable candidates for applications.

CRediT authorship contribution statement

Hemn Gharib Hussein: Writing - original draft, Visualization, Validation, Software, Resources, Methodology, Investigation, Formal analysis, Data curation. **Nzar Rauf Abdullah**: Writing, reviewing and editing – original draft, Validation, Investigation, Formal analysis, Supervision. **Vidar Gudmundsson**: Writing, review and editing – original draft, Validation, Investigation, Formal analysis, Supervision.

5. Acknowledgment

This work was financially supported by the University of Sulaimani. Part of the computational work was carried out using the resources of the Computational Nanoscience Laboratory at the Research and Development Center, University of Sulaimani. This study forms part of a PhD research project conducted at the University of Sulaimani.

References

[1] K. S. Novoselov, A. K. Geim, S. V. Morozov, D.-e. Jiang, Y. Zhang, S. V. Dubonos, I. V. Grigorieva, A. A. Firsov, Electric Field Effect in Atomically Thin Carbon Films, Science 306 (5696) (2004) 666–669.

[2] C. Lee, X. Wei, J. W. Kysar, J. Hone, Measurement of the Elastic Properties and Intrinsic Strength of Monolayer Graphene, Science 321 (5887) (2008) 385–388.

[3] J. Robertson, Diamond-like amorphous carbon, Materials Science and Engineering: R: Reports 37 (4–6) (2002) 129–281.

[4] J. Mahmood, E. K. Lee, M. Jung, D. Shin, H.-J. Choi, J.-M. Seo, S.-M. Jung, D. Kim, F. Li, M. S. Lah, et al., Two-dimensional polyaniline (C_3N) from carbonized organic single crystals in solid state, Proceedings of the National Academy of Sciences 113 (27) (2016) 7414–7419.

[5] J. Zeng, Z. Chen, X. Zhao, W. Yu, S. Wu, J. Lu, K. P. Loh, J. Wu, From all-triazine C_3N_3 Framework to Nitrogen-doped Carbon Nanotubes: Efficient and Durable Trifunctional Electrocatalysts, ACS Applied Nano Materials 2 (12) (2019) 7969–7977.

[6] I. Y. Kim, S. Kim, X. Jin, S. Premkumar, G. Chandra, N.-S. Lee, G. P. Mane, S.-J. Hwang, S. Umapathy, A. Vinu, Ordered Mesoporous C_3N_5 with a Combined Triazole and Triazine Famework and its Graphene Hybrids for the Oxygen Reduction Reaction (ORR), Angewandte Chemie 130 (52) (2018) 17381–17386.

[7] G. P. Mane, S. N. Talapaneni, K. S. Lakhi, H. Ilbeygi, U. Ravon, K. Al-Bahily, T. Mori, D.-H. Park, A. Vinu, Highly Ordered Nitrogen-rich Mesoporous Carbon Nitrides and Their Superior Performance for Sensing and Photocatalytic Hydrogen Generation, Angewandte Chemie International Edition 56 (29) (2017) 8481–8485.

[8] J. Shen, Q. Duan, J. Miao, S. He, K. He, W. Dai, C. Lu, New carbon–nitrogen–oxygen compounds as high energy density materials, Chinese Physics B 32 (9) (2023) 096302.

[9] J. Cui, S. Liang, X. Wang, J. Zhang, First principle modeling of oxygen-doped monolayer graphitic carbon nitride, Materials Chemistry and Physics 161 (2015) 194–200.

[10] P. Qiu, C. Xu, H. Chen, F. Jiang, X. Wang, R. Lu, X. Zhang, One step synthesis of oxygen doped porous graphitic carbon nitride with remarkable improvement of photo-oxidation activity: Role of oxygen on visible light photocatalytic activity, Applied Catalysis B: Environmental 206 (2017) 319–327.

[11] J. Huang, H. Wang, H. Yu, Q. Zhang, Y. Cao, F. Peng, Oxygen Doping in Graphitic Carbon Nitride for Enhanced Photocatalytic Hydrogen Evolution, ChemSusChem 13 (18) (2020) 5041–5049.

[12] F. T. Geldasa, F. B. Dejene, Transition metal doping effects on the structural, mechanical, electronic, and optical properties of α-NiS for photocatalysis applications via DFT+U insights, Applied Physics A 131 (11) (2025) 1–23.

[13] M. Jamal, S. S. Nishat, A. Sharif, Effects of transition metal (Fe, Co & Ni) doping on structural, electronic and optical properties of CuO: DFT+U study, Chemical Physics 545 (2021) 111160.

[14] H. Yoo, K. Heo, M. H. R. Ansari, S. Cho, Recent Advances in Electrical Doping of 2D Semiconductor Materials: Methods, Analyses, and Applications, Nanomaterials 11 (4) (2021) 832.

[15] H. Tian, Y. Lei, B. Sun, C.-C. Yang, C.-L. Chen, T. Huang, X. Zhang, Y. Chen, A. Song, L. Pang, et al., p–d orbital hybridization induced by transition metal atom sites for room-temperature sodium–sulfur batteries, National Science Review 12 (7) (2025) nwaf241.

[16] K. Badiane, G. Rodary, M. Amato, A. Gloter, C. David, H. Aubin, J.-C. Girard, Atomic-scale visualization of the p-d hybridization in III-V semiconductor surfaces doped with transition metal impurities, Physical Review B 105 (23) (2022) 235443.

[17] S. Belhachi, B. Merabet, S. Al-Qaisi, S. Goumri-Said, Exploring the Multifunctional Properties of Tm-doped $Al_xGa_{1-x}N$ alloys: From Photoluminescence to Spintronics, International Journal of Quantum Chemistry 124 (23) (2024) e27520.

[18] P. Wu, M. Huang, Transition metal doped arsenene: promising materials for gas sensing, catalysis and spintronics, Applied Surface Science 506 (2020) 144660.

[19] P. Li, Z. Zhang, Z. Zhuang, J. Guo, Z. Fang, S. L. Fereja, W. Chen, Pd-Doping-Induced Oxygen Vacancies in One-Dimensional Tungsten Oxide Nanowires for Enhanced Acetone Gas Sensing, Analytical Chemistry 93 (20) (2021) 7465–7472.

[20] S. N. Matussin, F. Khan, M. H. Harunsani, Y.-M. Kim, M. M. Khan, Effect of Pd-Doping Concentrations on the Photocatalytic, Photoelectrochemical, and Photoantibacterial Properties of CeO_2, Catalysts 13 (1) (2023) 96.

[21] M. Dhaouadi, M. Jlassi, I. Sta, I. B. Miled, G. Mousdis, M. Kompitsas, W. Dimassi, Influence of Pd-doping on structural, morphological, optical and electrical properties of sol–gel derived CuO thin films, Surfaces and Interfaces 17 (2019) 100352.

[22] P. Giannozzi, S. Baroni, N. Bonini, M. Calandra, R. Car, C. Cavazzoni, D. Ceresoli, G. L. Chiarotti, M. Cococcioni, I. Dabo, et al., QUANTUM ESPRESSO: a modular and open-source software project for quantum simulations of materials, Journal of Physics: Condensed Matter 21 (39) (2009) 395502.

[23] P. Giannozzi, O. Andreussi, T. Brumme, O. Bunau, M. Buongiorno Nardelli, M. Calandra, R. Car, C. Cavazzoni, D. Ceresoli, M. Cococcioni, et al., Advanced capabilities for materials modelling with Quantum ESPRESSO, Journal of Physics: Condensed Matter 29 (46) (2017) 465901.

[24] J. P. Perdew, K. Burke, M. Ernzerhof, Generalized Gradient Approximation Made Simple, Physical Review Letters 77 (18) (1996) 3865.

[25] H. Ehrenreich, M. H. Cohen, Self-Consistent Field Approach to the Many-Electron Problem, Physical Review 115 (4) (1959) 786.

[26] A. Kokalj, Computer graphics and graphical user interfaces as tools in simulations of matter at the atomic scale, Computational Materials Science 28 (2) (2003) 155–168.

[27] N. R. Abdullah, B. J. Abdullah, H. G. Hussein, V. Gudmundsson, Novel ZnO nanosheet with buckling stress: First principles study of electronic, structural stability, phonon vibrations, lattice thermal and

optical conductivity, Chemical Physics Letters 844 (2024) 141269.

[28] A. Togo, L. Chaput, T. Tadano, I. Tanaka, Implementation strategies in phonopy and phono3py, Journal of Physics: Condensed Matter 35 (35) (2023) 353001.

[29] A. Jehan, M. Husain, S. Bibi, N. Rahman, V. Tirth, A. Azzouz-Rached, M. Y. Khan, M. Nasir, K. Inayat, A. Khan, et al., Insight into the structural, optoelectronic, and elastic properties of $AuXF_3$ (X = Ca, Sr) fluoroperovskites: DFT study, Optical and Quantum Electronics 55 (14) (2023) 1242.

[30] H. G. Hussein, N. R. Abdullah, V. Gudmundsson, First-Principles Study of Structural, Electronic, Thermal, and Optical Properties of Quasi-2D C_2N_2O Using GGA and HSE06, arXiv preprint arXiv:2604.26149 (2026).

[31] H. van Gog, W.-F. Li, C. Fang, R. S. Koster, M. Dijkstra, M. van Huis, Thermal stability and electronic and magnetic properties of atomically thin 2D transition metal oxides, npj 2D Materials and Applications 3 (1) (2019) 18.

[32] X. Zhao, C. Yang, T. Wang, X. Ma, S. Wei, C. Xia, 3d transition metal doping-induced electronic structures and magnetism in 1T-$HfSe_2$ monolayers, RSC Advances 7 (83) (2017) 52747–52754.

[33] N. R. Abdullah, H. G. Hussein, V. Gudmundsson, DFT study of BN-codoped SrO monolayer: Interatomic interactions between dopant atoms control electronic, magnetic, thermal, and optical properties, Physica B: Condensed Matter 690 (2024) 416277.

[34] A. Togo, First-principles Phonon Calculations with Phonopy and Phono3py, Journal of the Physical Society of Japan 92 (1) (2023) 012001.

[35] C. M. Fang, G. A. De Wijs, Lattice vibrations and thermal properties of carbon nitride with defect ZnS structure from first-principles calculations, Journal of Physics: Condensed Matter 16 (18) (2004) 3027.

[36] T. Tohei, H.-S. Lee, Y. Ikuhara, First Principles Calculation of Thermal Expansion of Carbon and Boron Nitrides Based on Quasi-harmonic Approximation, Materials Transactions 56 (9) (2015) 1452–1456.